ELSEVIER

Journal of Physics and Chemistry of Solids 61 (2000) 969–977

JOURNAL OF PHYSICS AND CHEMISTRY OF SOLIDS

www.elsevier.nl/locate/jpcs

Study of linear and nonlinear optical properties of distorted Ti–O_6 perovskite structure in $Ba_xSr_{1-x}TiO_3$

W.K. Chen[a], C.M. Cheng[a], J.Y. Huang[a,*], W.F. Hsieh[a], T.Y. Tseng[b]

[a]*Institute of Electro-Optical Engineering, Chiao Tung University, Hsinchu, Taiwan, ROC*
[b]*Institute of Electronics, Chiao Tung University, Hsinchu, Taiwan, ROC*

Received 13 July 1999; accepted 21 September 1999

Abstract

We report the linear and nonlinear optical properties of sol–gel prepared $Ba_xSr_{1-x}TiO_3$ (BST) crystalline powders. The results from powder X-ray diffraction, birefringence, and second-order optical nonlinearity measurements indicate that the paraelectric–ferroelectric phase transition of $Ba_{0.75}Sr_{0.25}TiO_3$ occurs near room temperature. The second-order optical nonlinearity of the ferroelectric BST is about 7.9 pm/V. The index of refraction, $n = 2.2$, and birefringence, $\Delta n_B \sim 0.05$, are also appropriate for practical nonlinear optical applications.

Keywords: A. Optical materials; B. Sol–gel growth; D. Ferroelectricity; D. Optical properties; D. Phase transitions

1. Introduction

Ferroelectric materials possess useful properties, which relate to their field-reversible spontaneous polarization below the Curie temperature T_C. Two remanant polarizations with opposite polarity are available. The lower frequency transverse optical phonons of some ferroelectrics soften near the ferro–paraelectric phase transition [1] and give rise to highly nonlinear dielectric constant. Ferroelectric materials have been widely used in many applications ranging from sensors and actuators [2], new nonvolatile random access memory [3], to various microwave devices such as frequency-agile filters, phase shifters and tunable high-Q resonators [3–5]. An ideal material for these applications must possess high dielectric constant, low dielectric loss, and tunability in material properties.

Ternary and more complex oxides with perovskite structure such as $Ba_xSr_{1-x}TiO_3$ represent an important class of ferroelectric materials, whose electrical properties are tunable with their compositions and structures. Barium titanate ($BaTiO_3$) belongs to the displacement type of ferroelectric material, for which the origin of ferroelectricity derives from the displacement of ions relative to each other with a Curie temperature of 393 K [6], while $SrTiO_3$ is paraelectric and never becomes ferroelectric even at 0 K. It is known that the dielectric constant of $Ba_xSr_{1-x}TiO_3$ (BST) varies with $x = Ba/(Ba + Sr)$ and becomes anomalously large at the structural phase transition [7]. The mechanism giving rise to the giant dielectric constant has remained unclear. The large dielectric constant of BST thin films can also be tuned with an external electric field, which makes the material attractive for the development of various microwave devices [3].

The electrical properties of BST films had been subjected to detailed investigation, however little has been done to reveal their optical properties at various compositions [8]. Optical applications with BST are interesting as many advanced nonlinear optical devices with BST films can be realized by using the periodic poling technique [9,10].

This paper is organized as follows: in Section 2, we first describe the experimental procedure used to prepare BST samples. The measurement methods to be used for characterizing the linear and nonlinear optical properties are then given. The experimental results are presented in Section 3. Finally, in Section 4, the discussion is given and the conclusions drawn.

* Corresponding author.

0022-3697/00/$ - see front matter
PII: S0022-3697(99)00347-9

2. Experimental procedures

2.1. Preparation of BST powders with a sol–gel method

The sol–gel technique [11] was employed for preparing $Ba_xSr_{1-x}TiO_3$ crystalline powders in order to yield samples with high composition accuracy. We first boiled acetic acid to 120°C for producing dehydrated solvent. A proper amount of barium acetate and strontium acetate (99% purity from Gransman Inc.) was dissolved in dehydrated acetic acid at 90°C and was sufficiently stirred for 20 min. Titanium isopropoxide and some di-ethanol were then added to the solution and were stirred for another 20 min. We dried and solidified the solution by illuminating with a 400-W infrared lamp for two days. The resulting white solid was heated to 165°C for 1 h and then ground into powders. We then sintered the powders at 1000°C for 150 min.

The powders were pressed into pellets with a pressure of 10,000 psi and the pellets were sintered again at 1350°C. The surfaces of the resulting pellets were polished for measuring the indices of refraction and powder X-ray diffraction patterns. For powder SHG measurements, the pellets were ground and then sieved to obtain powder samples with particle sizes of 45, 60, 100, 140, 270 and 400 meshes.

2.2. Linear optical measurement

To rapidly test and screen a library of new nonlinear optical materials, it is highly desired to develop some simple methods for evaluating the linear and nonlinear optical properties of the powder samples.

Stagg and Charampopoulos [12] devised a technique for measuring the index of refraction, $\bar{n} = n - i\kappa$, of a powder sample. They found that the power reflectance from a rough surface at an incident angle, θ, can be described with

$$R(\bar{n}, \theta, \sigma/\lambda) = \rho(\theta, \sigma/\lambda) R_0(\bar{n}, \theta). \tag{1}$$

Here R_0 represents the reflectance from an ideal smooth surface, and ρ is the scattering factor from surface roughness. Assuming that the rough surface can be modeled with a surface profile that follows Gaussian distribution with a root-mean-squared (rms) roughness of σ/λ, the scattering factor can then be derived with Kirchhoff's scalar diffraction theory. For a surface with roughness $\sigma/\lambda < 1$ and correlation length $L_c/\lambda < 1$, the scattering factor can be simplified to a polarization-independent term [12]

$$\rho(\theta, \sigma/\lambda) = \exp\left[-\left(4\pi \cos\theta \frac{\sigma}{\lambda}\right)^2 \right]. \tag{2}$$

Therefore, the ratio of the two power reflectances with p- and s-polarized light becomes

$$r = \frac{R_p(\bar{n}, \theta, \sigma/\lambda)}{R_s(\bar{n}, \theta, \sigma/\lambda)} = \frac{R_{0,p}(\bar{n}, \theta)}{R_{0,s}(\bar{n}, \theta)}. \tag{3}$$

This ratio can be related to the complex index of refraction $\bar{n} = n - i\kappa$ of material by

$$r = \frac{a^2 + b^2 - 2a \sin\theta \tan\theta + \sin^2\theta \tan^2\theta}{a^2 + b^2 + 2a \sin\theta \tan\theta + \sin^2\theta \tan^2\theta}, \tag{4}$$

where

$$2a^2 = \sqrt{(n^2 - \kappa^2 - \sin^2\theta)^2 + 4n^2\kappa^2} + (n^2 - \kappa^2 - \sin^2\theta)$$

and

$$2b^2 = \sqrt{(n^2 - \kappa^2 - \sin^2\theta)^2 + 4n^2\kappa^2} - (n^2 - \kappa^2 - \sin^2\theta).$$

2.3. Characterization of second-order nonlinear optical properties

Kurtz and Perry [13] were the first to investigate the second-order NLO responses of crystalline powders. Considering a fundamental beam with wavelength λ normally incidents on a crystal plate with thickness L, the total second-harmonic intensity can be expressed as [14]

$$I_{2\omega} = \frac{128\pi^5 d_{\text{eff}}^2 I_\omega^2 L^2}{n_\omega^2 n_{2\omega} \lambda_{2\omega}^2 c} \frac{\sin^2[\Delta k L/2]}{[\Delta k L/2]^2}, \tag{5}$$

where $\Delta k = k(2\omega) - 2k(\omega)$, I_ω is the intensity of the incident fundamental beam, n_ω, $n_{2\omega}$ and d_{eff} are the indices of refraction and the effective nonlinearity of the crystal plate. When the plate is made with crystalline powders, the second-harmonic intensity becomes [15]

$$I_{2\omega} = \frac{512\pi^3 I_\omega^2 \bar{l}_c^2}{n_\omega^2 n_{2\omega} \lambda_{2\omega}^2 c} \langle d_{\text{eff}}^2 \rangle \frac{L}{r} \sin^2\left[\frac{\pi}{2} \left(\frac{\bar{r}}{\bar{l}_c} \right) \right]. \tag{6}$$

Here $\bar{r}$ denotes the averaged particle size, $\bar{l}_c = \langle \lambda_\omega / 4(n_{2\omega} - n_\omega) \rangle$ is the coherent length, and $\langle d_{\text{eff}}^2 \rangle$ the square of the effective nonlinearity averaged over the orientation distribution of crystalline powders. When the second-harmonic generation is not phase matchable, Eq. (6) leads to the following asymptotic forms [15]:

$$I_{2\omega} \rightarrow \begin{cases} \dfrac{128\pi^5 I_\omega^2}{n_\omega^2 n_{2\omega} \lambda_{2\omega}^2 c} \langle d_{\text{eff}}^2 \rangle L \cdot \bar{r}, & \bar{r} \ll \bar{l}_c, \\ \dfrac{256\pi^3 I_\omega^2 \bar{l}_c^2}{n_\omega^2 n_{2\omega} \lambda_{2\omega}^2 c} \langle d_{\text{eff}}^2 \rangle \dfrac{L}{\bar{r}}, & \bar{r} \gg \bar{l}_c \end{cases} \tag{7}$$

If the second-harmonic generation satisfies the type-I phase matching condition, we can rewrite Eq. (5) as [16]

$$I_{2\omega}(\bar{r}, \theta) = \frac{128\pi^5 \langle d_{\text{eff}}^2 \rangle I_\omega^2}{n_\omega^2 n_{2\omega} \lambda_{2\omega}^2 c} L \cdot \bar{r} \frac{\sin^2\left[\dfrac{\pi}{2} \dfrac{\bar{r}}{\bar{l}_{pm}} (\theta - \theta_{pm}) \right]}{\left[\dfrac{\pi}{2} \dfrac{\bar{r}}{\bar{l}_{pm}} (\theta - \theta_{pm}) \right]^2}, \tag{8}$$

where $\bar{l}_{pm} = \lambda_\omega / [4|\Delta n_{B,2\omega}| \sin 2\theta_{pm}]$, and θ_{pm} is the phase matching angle. Here $\Delta n_{B,2\omega} = n_{E,2\omega} - n_{O,2\omega}$ denotes the birefringence of material at the second-harmonic wavelength. In the event that $\bar{r} \gg \bar{l}_{pm}$ or $\bar{r} \ll \bar{l}_{pm}$, Eq. (8) can

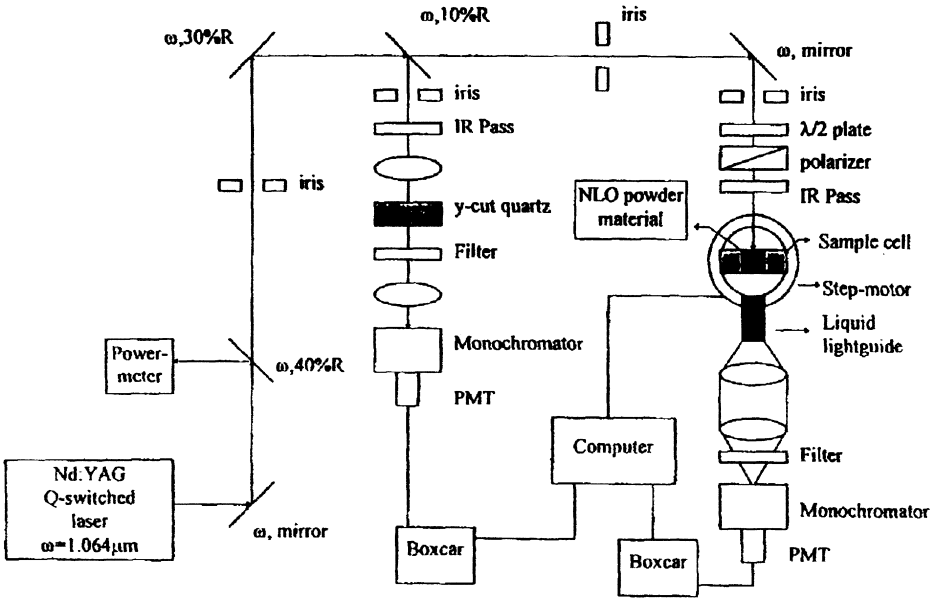

Fig. 1. Experimental setup used for measuring the second harmonic scattering pattern from a crystalline powder sample.

be simplified to

$$I_{2\omega} \rightarrow \begin{cases} \dfrac{256\pi^4 I_\omega^2}{n_\omega^2 n_{2\omega} \lambda_{2\omega}^2} \langle d_{\text{eff}}^2 \rangle L \cdot \bar{l}_{\text{pm}}, & \bar{r} \gg \bar{l}_{\text{pm}}, \\ \dfrac{128\pi^5 I_\omega^2}{n_\omega^2 n_{2\omega} \lambda_{2\omega}^2} \langle d_{\text{eff}}^2 \rangle L \cdot \bar{r}, & \bar{r} \ll \bar{l}_{\text{pm}} \end{cases} \tag{9}$$

We derived a useful empirical formula, which possesses the correct asymptotic forms in Eq. (9), to depict the overall variation in second harmonic intensity with particle size $\bar{r}$

$$I_{2\omega} = I_0 \sqrt{1 - \exp[-(\bar{r}/A)^2]} \tag{10}$$

with

$$I_0 = \frac{256\pi^4 I_\omega^2}{n_\omega^2 n_{2\omega} \lambda_{2\omega}^2 c} L \bar{l}_{\text{pm}} \langle d_{\text{eff}}^2 \rangle$$

and

$$A \approx 9\bar{l}_{\text{pm}}.$$

An experimental arrangement for measuring the second-harmonic scattering pattern from crystalline powders is described in Fig. 1. In this setup, the fundamental beam normally incidents on the sample cell. A liquid light guide with its input end attached on a rotation stage is employed to collect the second harmonic intensity at various scattering angles. We can integrate the second harmonic pattern over scattering angle to yield the total second harmonic intensity, $I_{2\omega}$.

3. Results

3.1. Structural determination of $Ba_xSr_{1-x}TiO_3$ with powder X-ray diffraction

It had been revealed that the mechanical, electrical and optical properties of solid solutions of $Ba_xSr_{1-x}TiO_3$ strongly depend on the mole fraction of Ba. We are therefore interested in studying the structures of BST perovskites with accurately controlled Ba compositions.

We first employ X-ray diffraction (XRD) for probing the unit cell dimensions of $Ba_xSr_{1-x}TiO_3$ with various x-values. The resulting XRD patterns were then analyzed with the Rietveld refinement procedure [17]. In Fig. 2, the XRD patterns from four powder samples ($x = 1$, 0.8, 0.5 and 0, from top to bottom) are presented. The averaged cell dimension as a function of x is summarized in Fig. 3.

The unit cell of our synthesized $BaTiO_3$ crystalline powder has an averaged dimension of $(a + c)/2 = (3.986 + 4.020)/2 = 4.003$ Å. The data agrees well with the published results, where a is found to range from 3.9915 to 3.9998 Å and c from 4.018 to 4.025 Å) (for $BaTiO_3$ (P4MM) see Refs. [18,19]). For $SrTiO_3$, our measured result ($a = b = c = 3.897$ Å) is slightly smaller than the published data (a varies from 3.900 to 3.905 Å) (for $SrTiO_3$ (PM-3M) see Refs. [20,21]), but the difference is within our experimental error. It can also be seen that Vegard's linear scaling law [8] is satisfied only within $0.2 < x < 0.7$. Outside the range, the cell dimension does not change significantly with x.

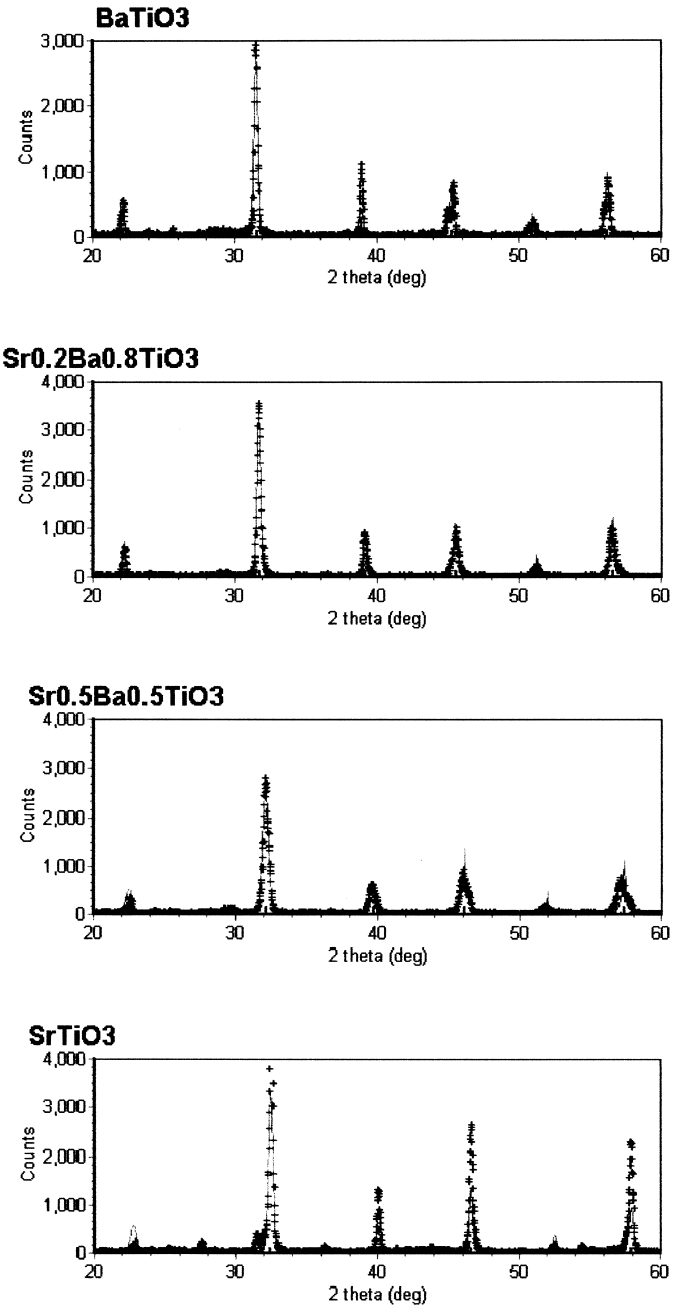

Fig. 2. Powder X-ray diffraction patterns (symbols) of $Ba_xSr_{1-x}TiO_3$ with $x = 1$, 0.8, 0.5 and 0 (from top to bottom). The solid curves are ones that have resulted from the Rietveld refinement procedure.

3.2. Linear optical properties of $Ba_xSr_{1-x}TiO_3$

To estimate the measuring accuracy of the index of refraction from Eq. (4), we first apply this linear optical technique on some well-known NLO materials. The results of KH_2PO_4 (KDP) crystalline powder at $\lambda = 0.633\ \mu m$ are presented in Fig. 4. By using Eq. (4), the index of refraction of KDP was determined to be 1.49, which is fairly close to the averaged value of n_E and n_O of KDP single crystal (see Table 1) [22].

We then apply this method to probe linear optical properties of BST powders with various Ba/(Ba + Sr) ratios. The

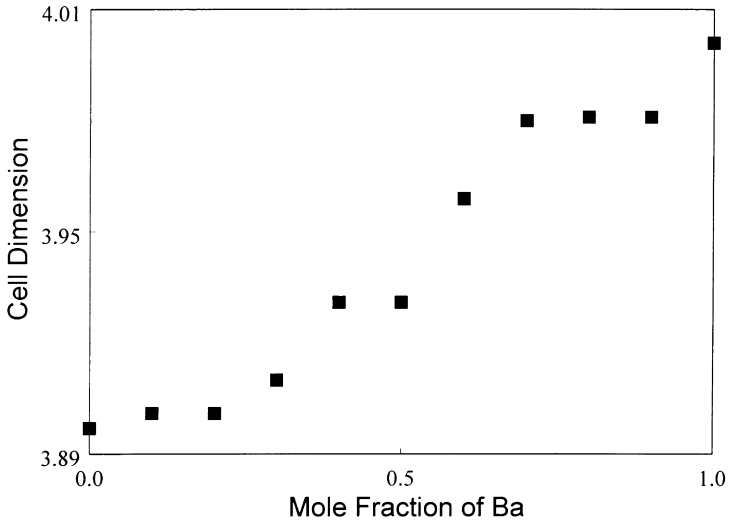

Fig. 3. Averaged unit cell dimension, $(a + c)/2$, deduced from the Rietveld refinement procedure is plotted as a function of x. The point group symmetry of the unit cell is taken to be C_{4v} for $x \geq 0.75$ and O_h for $x < 0.75$.

results are presented in Fig. 5, which show that the index of refraction of BST is fairly constant (~2.20). The value is about 8% lower than that taken from single crystal $BaTiO_3$ ($n_{av} = 2.39$) and $SrTiO_3$ ($n = 2.39$) [23]. The deviation is most likely to have originated from the larger light scattering loss from our powder samples.

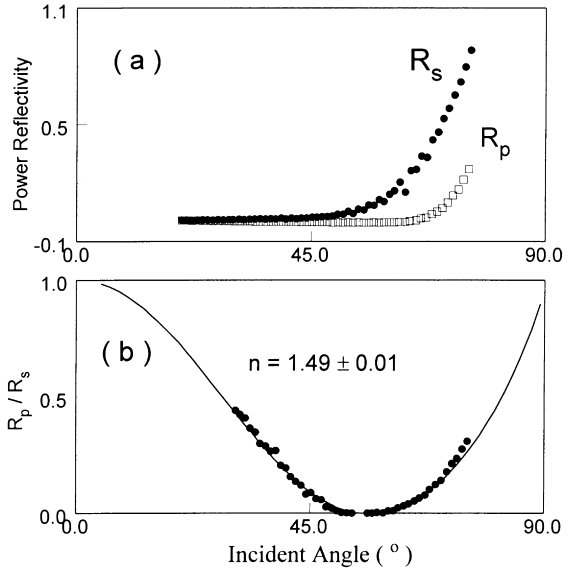

Fig. 4. (a) Power reflectances with s- (filled symbols) and p-polarized (open squares) beams as a function of incident angle from a KDP powder pellet. (b) The ratio of the power reflectances with the p-polarized to s-polarized incident beams is presented (symbols). The solid curve is the theoretical fit to Eq. (4) with $n = 1.49$ and $\kappa = 0$.

3.3. Nonlinear optical properties of $Ba_xSr_{1-x}TiO_3$

For calibration, the nonlinear optical (NLO) characterization apparatus described in Fig. 1 was first applied to investigate NLO responses of KDP and β-BaB_2O_4 (BBO) powders. The results show that second harmonic generation from these two standard materials is phase matchable at 1.06 μm. The NLO response from BBO is about four times that of KDP, which agrees very well with the published values [22].

We then apply this experimental setup to measure NLO properties of BST powders. The results are shown in Fig. 6. The second harmonic generation from BST is also phase matchable at 1.06 μm. The effective second-order nonlinearities of $Ba_xSr_{1-x}TiO_3$ with $x = 0.8$ and 0.7 were found to be about 7.2 and 3.5 pm/V, respectively. The effective nonlinearities, $\sqrt{\langle d_{\text{eff}}^2 \rangle}$, and birefringence, $\Delta n_B = n_{E,2\omega} - n_{O,2\omega}$, of BST with various x are summarized in Fig. 7. It is interesting to note that the $\sqrt{\langle d_{\text{eff}}^2 \rangle}$ and Δn_B exhibit a discontinuous change with $x = 0.75$. This supports that BST with Ba/(Ba + Sr) ~ 0.75 undergoes a structural phase transition near room temperature. Table 1 summarizes our results of the optical properties of KDP, BBO and BST.

4. Discussion and conclusions

From the XRD patterns shown in Fig. 2, we found that the peaks near 45 and 51° are split into two neighboring subpeaks when the ratio of Ba/(Sr + Ba) is higher than 0.7. To further reveal the origin of the splittings, we perform XRD simulations on $BaTiO_3$ with a crystal structure of *P*4*MM* (C_{4v}) and *PM*-3*M* (O_h).

The simulated results, which are shown in Fig. 8, indicate

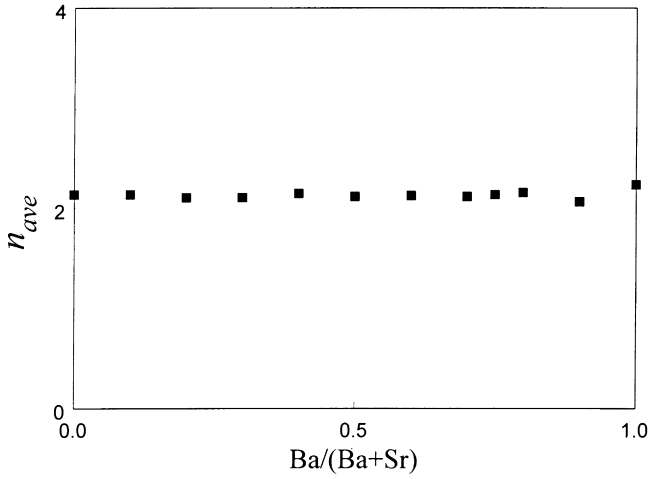

Fig. 5. The measured index of refraction of $Ba_xSr_{1-x}TiO_3$ is presented as a function of $_x$.

that the structural change of unit cell can cause the atomic plane spacing in {200} (corresponding to $2\theta \sim 45°$) to be different. The similar behavior also happens in {210} ($2\theta \sim 50°$). Thus the observed splittings in our XRD patterns provide a direct evidence of a structural change from O_h to C_{4v} in BST when Ba/(Ba + Sr) is higher than 0.75.

As pointed out previously barium titanate ($BaTiO_3$) belongs to the displacement type of ferroelectric material for which the origin of ferroelectricity derives from the displacement of ions relative to each other. It is believed that BST undergoes the same sequence of structural phase transitions as pure $BaTiO_3$ does, but at progressively lower phase transition temperatures as the concentration of Ba is reduced. The $Ti-O_6$ octahedron in the ferroelectric $BaTiO_3$ is distorted with C_{4v}-symmetry. The resulting spontaneous polarization, P_s, can be expressed as [24]

$$P_s = P_0' \cdot \Delta z, \tag{11}$$

where Δz denotes the displacement of ions from the symmetric positions which are occupied in the paraelectric phase. P_s serves as an order parameter of the phase transition and therefore above the transition the parameter varies with temperature by [25]

$$P_s = a\sqrt{T_c - T}. \tag{12}$$

Recently, Wang [26] had proposed a simple two-band model suited for describing polarization in a ferroelectric crystal. With the model, the second-order NLO coefficient

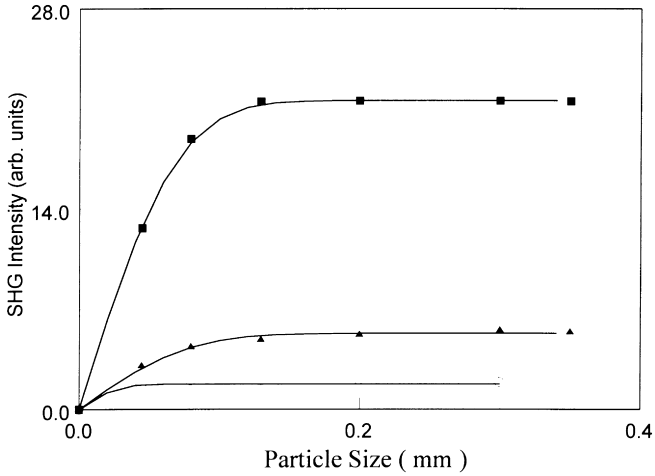

Fig. 6. Effective second-order optical nonlinearities of BBO (open circles), $Ba_xSr_{1-x}TiO_3$ ($x = 0.7$, filled triangles) and $Ba_xSr_{1-x}TiO_3$ ($x = 0.8$, filled squares) are plotted as a function of particle size. The solid curves are the theoretical fit to Eq. (10).

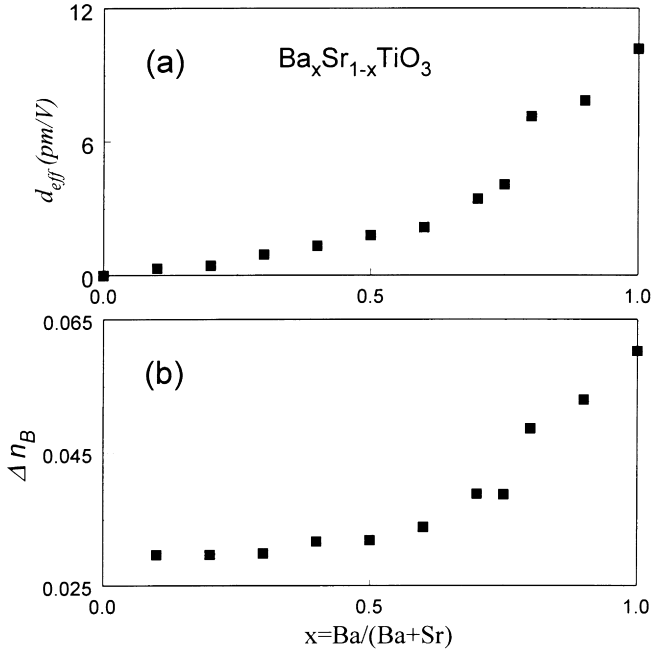

Fig. 7. The measured $\sqrt{\langle d_{\text{eff}}^2 \rangle}$ and Δn_{B} of $Ba_xSr_{1-x}TiO_3$ are plotted as a function of x.

of a ferroelectric crystal had been derived to be

$$d_{\text{eff}} = \frac{\pi C(n_\omega^2 + 2)^2 E_0^6}{18(E_0^2 - \hbar^2\omega^2)^2(E_0^2 - 4\hbar^2\omega^2)} P_{\text{s}}. \tag{13}$$

Here E_0 is the energy gap of the ferroelectric material and C denotes a simple constant. By combining Eqs. (11) and (13), we then have

$$d_{\text{eff}} = d' \cdot \Delta z. \tag{14}$$

Note that the displacement of ions may lead to a change in unit cell dimension. Based on the model, birefringence can also be related to spontaneous polarization by $\Delta n_{\text{B}} = B \cdot P_{\text{s}}^2$ [26]. Therefore, we are expecting to observe that both the second-order optical nonlinearity and birefringence vary with the mole fraction of Ba. Indeed, this is what we have observed, as shown in Fig. 7.

We should point out that the linear optical dispersion from 1.064 to 0.532 μm in a single crystal $BaTiO_3$ is about 0.13 [23], which is larger than the birefringence ($\Delta n_{\text{B}} = -0.06$). Therefore the type-I phase matching condition should not be satisfied in $BaTiO_3$ at 1.064 μm.

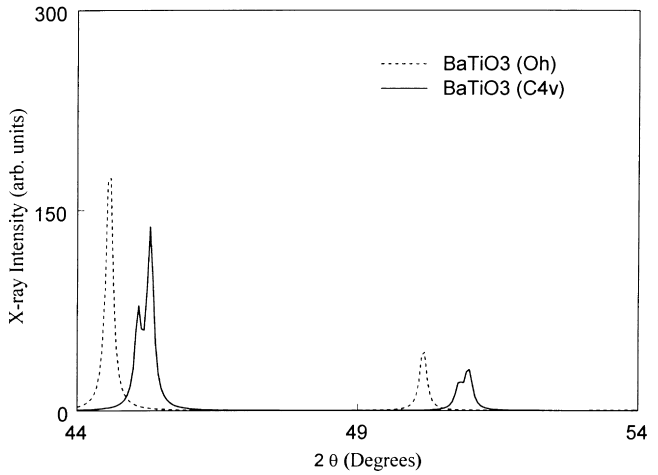

Fig. 8. Calculated powder X-ray patterns $BaTiO_3$ crystalline powder with a point group symmetry of O_h (dashed curve) and (b) C_{4v} (solid curve).

Table 1
Linear and second-order nonlinear optical properties of some crystalline powders

	Refractive indices of crystal at 0.633 μm	Second-order nonlinearity of crystal at 1.064 μm	n (0.633 μm)	l_{pm} (μm)	Δn_B (0.532 μm) $= \lvert n_E - n_O \rvert$	d_{eff}/d_{eff} (KDP) @ 1.064 μm	d_{eff} (pm/V) @ 1.064 μm
KDP	$n_O = 1.512$ $n_E = 1.417$ $n_{av} = 1.492$ $\Delta n_B = -0.041$	$d_{36} = 0.39$ $d_{eff}(I) = d_{36} \sin\theta \sin\phi$	1.49	11.1	0.04	1.0	0.4
β-BBO	$n_O = 1.675$ $n_E = 1.555$ $n_{av} = 1.615$ $\Delta n_B = -0.120$	$d_{22} = 2.22$ $d_{31} = 0.16$ $d_{eff}(I) = d_{31} \sin\theta - d_{22} \cos\theta \sin 3\phi$	1.58	3.7	0.13	4.0	1.5
$Ba_{0.7}Sr_{0.3}TiO_3$			2.12	13.0	0.04	9.3	3.5
$Ba_{0.8}Sr_{0.2}TiO_3$			2.16	9.7	0.05	19.3	7.2

However, note that the single crystal $BaTiO_3$ usually contains various transition metal impurities, which often results in red shift of the absorption edge. Our BST crystalline powders prepared with the sol–gel method do not contain such unintended dopants. Therefore our samples more accurately reflect the intrinsic properties of the materials and possess smaller dispersion in the visible light spectrum region. This can lead to the observed type-I phase matched second-harmonic generation in BST, as shown in Fig. 6.

Note that the index of refraction at the zero frequency limit ($\hbar\omega \ll E_0$) can be expressed as [27]

$$n^2 = 1 + \frac{8\pi e^2\hbar^2}{m^2 V} \sum_k \sum_{vc} \frac{p_{vc}(k)p_{cv}(k)}{E_{cv}^3(k)}. \quad (15)$$

It is dominated by those interband transitions which lie near band gap (smaller E_{cv}) and possess large momentum matrix elements, p_{cv}. In BST, oxygen's 2p and titanium's 3d orbitals dominate these transitions, where Ba and Sr do not play an important role. This indicates that the index of refraction of BST should be irrelevant to the concentration of Ba. Indeed this is exactly what we discover in Fig. 5. It should be pointed out that Ba/Sr play the major role in causing unit cell distortion, which more sensitively reflects in second-order optical nonlinearity and birefringence.

The birefringence of BST shown in Fig. 7 varies from 0.03 to 0.06 as the mole fraction of Ba is increased from 0 to 1. Note that to achieve high conversion efficiency both the phase matching condition ($\Delta k = 0$) and the large angular acceptance $\delta\theta \approx 0.443\lambda_\omega/(L|\Delta n_B|)$) have to be achieved. The measured linear and nonlinear optical properties of BST warrant a high efficacy in second-order nonlinear optical applications.

In summary, we investigate linear and nonlinear optical properties of $Ba_xSr_{1-x}TiO_3$ with various mole fractions of Ba. Our results indicate ferroelectric BST possess an effective second-order nonlinearity of about 7.9 pm/V, which is comparable to $LiNbO_3$. In addition, the index of refraction, $n = 2.2$, and birefringence, $\Delta n_B \sim 0.05$, are also appropriate for practical NLO applications. By combining with their excellent electrical and mechanical characteristics, BST could serve as an ideal multifunctional, smart material in micro optical electro-mechanical systems (MOEMS) [28,29].

Acknowledgements

We acknowledge the financial support from the National Science Council of the Republic of China under grants No. NSC87-2115-E-009-008 and NSC 87-2112-M-009-028.

References

[1] E.C.S. Tavares, P.S. Pizani, J.A. Eiras, Appl. Phys. Lett. 72 (1998) 987.
[2] J.M. Herber, Ferroelectric Transducers and Sensors, Gordon and Breach, London, 1982.
[3] J.F. Scott, Ferroelectr. Rev. 1 (1998) 1.
[4] L.A. Knauss, J.M. Pond, J.S. Horwitz, D.B. Chrisey, Appl. Phys. Lett. 69 (1996) 25.
[5] P. Bhattacharya, T. Komeda, K. Park, Y. Nishioka, Jpn. J. Appl. Phys., Part 1 32 (1993) 4102.
[6] H.P. Roaksby, H.D. Megaw, Nature 155 (1945) 484.
[7] F.N. Bunting, G.R. Shelton, A.S. Creamer, J. Am. Ceram. Soc. 30 (1947) 114.
[8] P. Pasierb, S. Komornicki, M. Radecka, Thin Solid Films 324 (1998) 134.
[9] L.E. Myers, G.D. Miller, R.C. Eckardt, M.M. Fejer, R.L. Byer, W.R. Bosenberg, Opt. Lett. 20 (1995) 52.
[10] H. Karisson, F. Laurell, L.K. Cheng, Appl. Phys. Lett. 74 (1999) 1519.
[11] L.L. Hench, J.K. West, Chem. Rev. 90 (1990) 33 072.
[12] B.J. Stagg, T.T. Charalampopoulos, Appl. Opt. 30 (1991) 4113.
[13] S.K. Kurtz, T.T. Perry, J. Appl. Phys. 39 (1968) 3798.
[14] R.W. Boyd, Nonlinear Optics, Academic Press, Boston, MA, 1992.
[15] A. Graja, Acta Phys. Polonica A 37 (1970) 539.
[16] P.N. Prasad, D.J. Williams, Introduction to Nonlinear Optical Effects in Molecules and Polymers, Wiley, New York, 1991 chap. 6.
[17] C.J. Howard, B.A. Hunter, A computer program for Rietveld analysis of X-ray and neutron powder diffraction patterns, Australian Nuclear Science and Technology Organization, Lucas Heights Research Laboratories, Private Mailbag 1, Menai 2234, NSW, Australia, February 1997.
[18] R. Waesche, W. Denner, H. Schulz, Mater. Res. Bull. 16 (1981) 497.
[19] R.H. Buttner, E.N. Maslen, Acta Crystallogr. B 48 (1992) 764.
[20] Y.A. Abramov, V.G. Tsirelson, V.E. Zavodnik, S.A. Ivanov, I.D. Brown, Acta Crystallogr. B 51 (1995) 942.
[21] S.A. Howard, J.K. Yau, H.U. Anderson, J. Appl. Phys. 65 (1989) 1492.
[22] V.G. Dmitriev, G.G. Gurzadyan, D.N. Nikogosyan, Handbook of Nonlinear Optical Crystals, Springer Series in Optical Sciences, 64, Springer, Berlin, 1991.
[23] E.D. Palik, Handbooks of Optical Constants of Solids II, Academic Press, San Diego, CA, 1991, pp. 789–804 see also pp. 1035–1048.
[24] W. Zhong, R.D. King-Smith, D. Vanderbilt, Phys. Rev. Lett. 72 (1994) 3618.
[25] G.A. Smolensky, J. Phys. Soc. Jpn 28 ((suppl.)) (1970) 26.
[26] F. Wang, Phys. Rev. B 59 (1999) 9733.
[27] B. Adolph, V.I. Gavrilenko, K. Tenelsen, F. Bechstedt, R. Del, Sole, Phys. Rev. B 53 (1996) 9797.
[28] A.W. Sleight, J.L. Gillson, P.E. Bierstedt, Solid State Commun. 17 (1975) 27.
[29] P.F. Baude, C. Ye, D.L. Polla, Appl. Phys. Lett. 64 (1994) 2670.